

Chapter 2

Experimental Methods

The techniques and equipment used for the characterization of the materials (at the molecular and macroscopic level) that have been used in this thesis are detailed below. Besides, the procedures used to modify the properties of the polymers of the study, mainly based on optical and thermal treatments, are also explained.

2.1 Sample Preparation

2.1.1 *Synthesis and Basic Characterization of the Materials*

The Department of Organic Chemistry of the University of Zaragoza took care of the synthesis of the molecules and polymers used in this thesis. Prof. Garín's group synthesized the highly efficient NLO chromophores whose hyperpolarizability in solution were measured as explained in [Chap. 3](#), whereas the Liquid Crystal and Polymer group was responsible for the monomer and polymer synthesis of the research. Both groups belong to the Institute of Materials Science of Aragon (ICMA—Instituto de Ciencia de Materiales de Aragón).

The chemical structure of the synthesized compounds was confirmed by infrared spectroscopy techniques and ^1H NMR. The particular features of its mesomorphic nature, as well as the thermal properties, were studied by means of differential scanning calorimetry and electronic microscopy. The molecular weights were determined by gel permeation chromatography (GPC).

The monomeric units of the main polymer of this research, Pol-PZ-CN (see [Fig. 4.1](#)), were prepared by azo-coupling of *N*-(hydroxyhexyl)-*N'*-phenylpiperazine with the 4-cyanoaniline diazonium salt. The radical polymerizations, thermally initiated by AIBN (azobis(isobutyronitrile)), were carried out in DMF (dimethylformamide) kept at a temperature of 70 °C [[1](#)].



Fig. 2.1 Azopolymer films and mixtures of polymers with chromophores prepared by free evaporation of CH_2Cl_2

2.1.2 Film Preparation and Thickness Measurement

The polymer films were produced by “casting” followed by free evaporation of the solvent. A small amount of the polymer (1–3 mg) was dissolved in 0.8 ml of filtered dichloromethane (CH_2Cl_2) and placed on three glass or fused silica substrates, with a surface of $2 \times 2 \text{ cm}^2$. The thickness and quality of the films obtained in this way depend on the concentration of the solution and the rate of evaporation of the solvent, among other things, so several concentrations were tested until transparent and homogeneous films of about $0.5 \text{ }\mu\text{m}$ thickness were obtained for some studies and in the range of $1\text{--}2 \text{ }\mu\text{m}$ for others.

In order to produce the non-centrosymmetric orientation needed for second harmonic signal generation, a corona discharge on the sample was used. The substrates used in these measurements had one of their faces coated with a $\cong 100 \text{ }\text{\AA}$ thick layer of ITO (indium tin oxide), which is a transparent conductor. Fused silica substrates (Qu-Suprasil) are also used for the optical absorption and refractive index measurements.

Substrate cleaning is a major necessity in order to obtain homogeneous films of good optical quality. The substrates underwent cleaning by sonication in several steps, following a protocol in which distilled water, soap and finally methanol were used. After that, they were subjected to UV irradiation in an ozone photoreactor. This method removes, by oxidation, any organic residues that may be on the surface, such as water or traces of solvent, grease from the skin or simply pollutants that might have stuck during prolonged exposure to air.

Once the glass was clean, the solution deposition of the concerned polymer was performed. In order to remove possible traces of solvent, the films were kept covered at 40°C on a hotplate for 12 h. In Fig. 2.1, a group of films that were part of the research in this thesis are shown. These films were prepared on glass substrates with ITO, as has been explained, and are composed of azopolymers, PMMA and mixtures of these with donor- π -acceptor chromophores.

It is necessary to know the thickness of the films in order to calculate the second-order nonlinear optical coefficients. To obtain the thickness two independent methods were used. One of the measurements was obtained using a contact profilometer Veeco Dektak³ST, which also allowed the surface relief of the samples to be measured, with a vertical nominal resolution in the range of nanometres along a straight line of up to 50 mm length. In practice, in good quality films, up to 5 nm can be discerned. Previous to the measurement, a groove was made in the film with a bradawl, thus crossing through its thickness to get to the other surface of the substrate while avoiding notching it. The measurement was carried out using a needle with a 2.5 μm radius diamond point, which scanned the surface film. The irregularities of the sample make the needle move vertically, sending an electric sign to the differential transformer that is coupled to it. In these measurements, the strength that the point makes on the film can be controlled in order not to damage it. In our case, we worked with the minimum one, 10 mg.

2.2 Optical Measurements

In this optical measurements section, the basic characterization techniques of the linear optical properties, as well as other techniques more specifically used to obtain the parameters quantifying the nonlinear response at the molecular and macroscopic scale of the studied materials, are included.

2.2.1 Optical Absorption Spectroscopy (UV-vis-NIR)

As a preliminary step to the measurements of SHG, not only in the chromophores in solution but also in the polymer films, it is necessary to know the absorption spectrum. This limits, for example, the wavelengths that can be used in the NLO measurements. Besides, in the case of films, the absorption measurements give information on the molecule ordering in the films, degree of aggregation, etc.

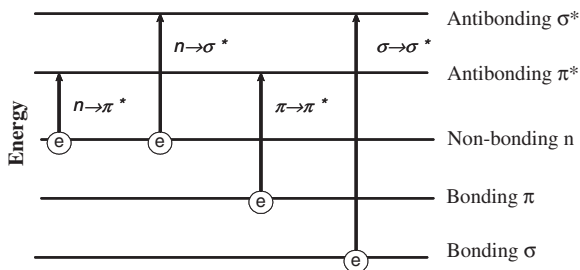
2.2.1.1 Theoretical Basis

By using optical absorption spectroscopy, the transitions between electronic states involving the external electrons of a system are studied. In the case of organic compounds, the UV and visible radiation absorption is restricted to certain functional groups, with valence electrons of low excitation energy.

These transitions entail a change in the electronic distribution, which leads to relatively wide absorption bands. In Fig. 2.2, a scheme of the different types of transitions occurring between the π , σ and n molecular orbitals is shown.

Among the schematic transitions in Fig. 2.2, the $n \rightarrow \pi^*$ and $\pi \rightarrow \pi^*$ ones constitute the basis of the absorption spectroscopy of organic compounds. These transitions need an unsaturated group in the molecule to deliver π electrons. The

Fig. 2.2 Electronic transitions for π , σ and n electrons



maxima for these transitions fall in the region of the visible spectrum, between 400 and 700 nm.

Solvent Effect. The energy of the schematized orbitals in Fig. 2.2 changes with the polarity of the medium. Therefore, the absorption spectrum of the molecules depends on the solvent in which it is measured. If we focus on the $\pi - \pi^*$ transitions, the interaction between the solvated molecule and the solvent is translated into a decrease of the energy in the fundamental and excited levels, which is usually clearer in the last one, so a shift of the corresponding band to a lower energy (a bathochromic shift, i.e. to longer wavelengths) can be seen, giving rise to positive solvatochromism, as explained in Chap. 1. These interactions, between molecule and solvent, increase with the polarity of the latter.

Absorption coefficient. When a solution reaches an intensity I_0 , the intensity transmitted can be expressed as $I_t = I_0 \times 10^{-OD}$, where OD is the absorbance of the sample. The absorbance or optical density, A , is directly proportional to the optical path l and the concentration of the absorbing species c . The Beer–Lambert law states that

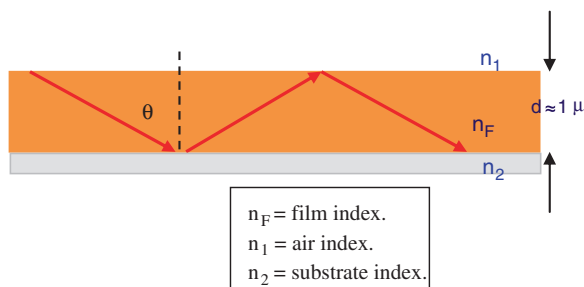
$$A = \varepsilon cl,$$

where ε is a constant of proportionality called absorptivity or absorption coefficient. During this work, for some compounds, it was necessary to calculate this absorption coefficient at different wavelengths, to make the relevant absorption corrections in the $\mu\beta$ values experimentally obtained by EFISH.

2.2.1.2 Experimental Setup

The optical absorption measurements were performed with a Varian Cary-500 UV–vis–NIR spectrophotometer, which measures the intensity I_t of the light transmitted by the sample as a function of the wavelength. It is a double beam spectrophotometer, which uses a tungsten halogen lamp as an exciter for wavelengths over 350 nm and a deuterium arc lamp for the UV. The wavelength is selected using a double monochromator with 0.05 nm resolution. The beam is divided into two, one reference beam and one that crosses the sample, and then the respective light intensities transmitted by the sample and the reference are compared.

Fig. 2.3 Representation of light propagation in a plane waveguide (polymer film)



Detection in the UV–vis range is by means of a photomultiplier and in the near IR with a PbS detector.

The wavelengths that were used with the polymer films ranged from 200 to 800 nm, except for the mixtures, in which the range extended up to 1200 nm. If ITO glass substrates are used, only wavelengths down to 300 nm can be reached, as the glass absorbs a lot under that value. For the particular case of some solutions of nonlinear chromophores, the range was also increased to frequencies in the near IR.

The measurements were made with non-polarized light and linearly polarized light. For the measurements with linearly polarized light, a Glan–Thompson prism was placed in the beam of the sample. On the other hand, the incorporation of a mount that could be rotated around a vertical axis allowed measurements to be made at an angle different to normal incidence.

2.2.2 Refractive Index Measurement

It is necessary to know the values of the refractive indices of the films at 1.91 μm and 953 nm for the further calculation of the nonlinear coefficients. Besides, knowing the n_x , n_y , and n_z refractive indices allows us to characterize the chromophore ordering in the film.

2.2.2.1 Theoretical Basis

In order to measure the refractive indices and the thickness of the polymer films, a technique based on light guiding with the film acting as a waveguide is used. The method is based on the fact that the light can be confined in a narrow transverse region with a refractive index higher than that of its surrounding medium and then guided through the medium by consecutive internal total reflections at its boundaries (Fig. 2.3). For a given wavelength of the incident light, thickness and index of the film, the light is only guided for certain values of the angle θ (propagating modes).

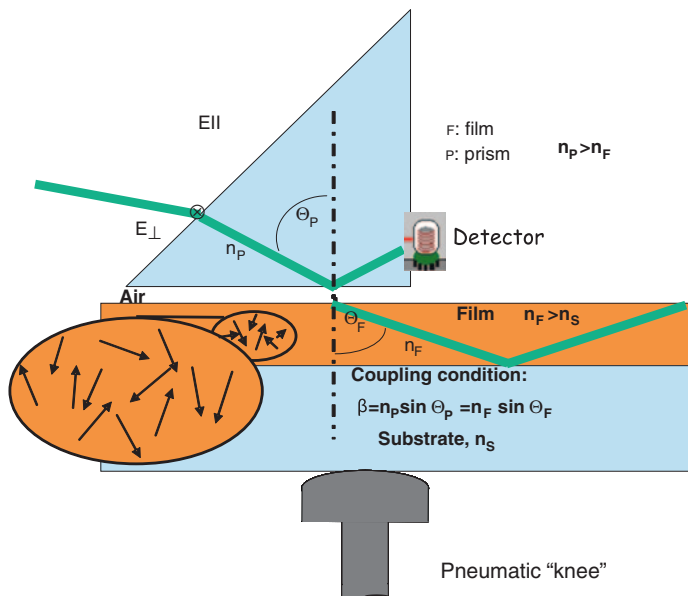


Fig. 2.4 Scheme of the experimental light prism coupling system in the film to measure the refractive indices

The propagating modes are classified as TE (transverse electric) or TM (transverse magnetic), depending on whether the incident light is polarized perpendicular or parallel to the incident plane. Once the angles at which the light is guided for the two polarizations are known, it is possible to deduce the values of the refractive indices: n_{TE} for the light polarized in the direction parallel to the plane of the film and n_{TM} perpendicular to it. For example, in the case of electric-field-oriented polymeric uniaxial films, where a Z optical axis is defined (Fig. 2.6) perpendicular to the film plane, the ordinary index $n_o = n_x = n_y$ will be measured as n_{TE} and the extraordinary one, $n_e = n_z$, will be deduced from the magnetic guided modes.

2.2.2.2 Experimental Setup

The refractive indices were measured using Metricon 2010 equipment, which includes a prism-coupled guided modes instrument.

The film, on a glass or quartz substrate, is placed in contact with the base of a prism through a pneumatic “knee”, whose force on the film can be controlled by varying the pressure of the compressed air (Fig. 2.4). Nevertheless, sometimes it is necessary to increase that pressure, so for this purpose a mechanic clamp that is controlled manually was designed. Once the light coupling into the film has been achieved by using the right pressure and correct focusing of the laser beam, the process is completely automated. The film/prism arrangement is rotated so that the angle of the incident light is changed and the detected intensity is registered as a function of the angle.

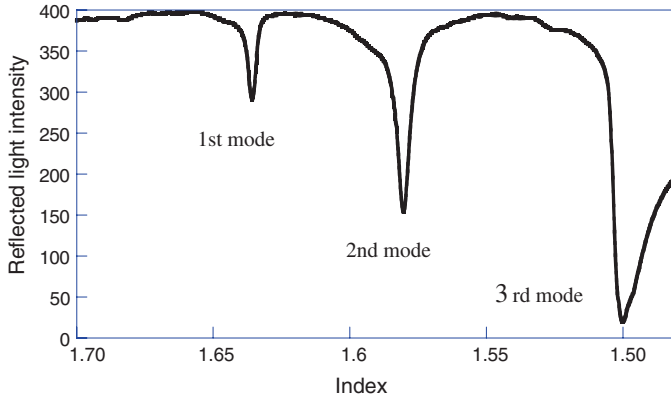


Fig. 2.5 Reductions in light intensity detected occur for angles at which the coupling condition is fulfilled

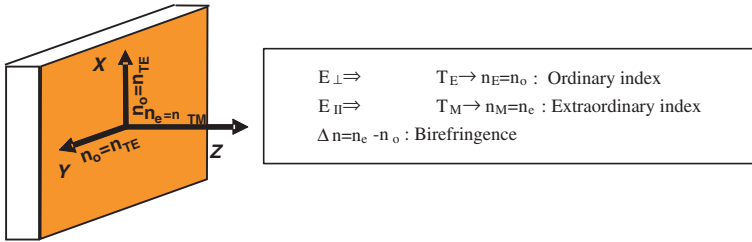


Fig. 2.6 Definition of the ordinary and extraordinary indices with respect to the film axes

The laser beam, after striking the prism and reflecting completely at the surface of the film, reaches the detector except for certain discrete values of the incidence angle, where the propagating modes are located. For these values of the angle, the light penetrates the film in wave guiding propagation mode. When this happens, that is, when the coupling condition is fulfilled, the detector registers an intense decrease of the light intensity reaching it. Figure 2.5 shows the typical guided modes record, which corresponds to the rough decrease of the light intensity that reaches the detector.

As soon as the modes are found, the equipment calculates the index and the thickness using an algorithm [2]. The angle at which the first mode is located and the angular separation between the modes allow the index and thickness of the film to be obtained. The coupling of two modes is therefore enough to determine uniquely the indices and the thickness.

The out-of-plane birefringence of the films, which will be referred to throughout this thesis, is the difference $\Delta n = n_{TM} - n_{TE}$. Therefore, n_o is the index in any direction in the film plane and n_e in the normal direction, as shown in Fig. 2.6.

The number of modes that can be guided increases with the film thickness. Films of at least 100–200 nm thickness are needed in most film/substrate combinations, so that the first mode can be seen at 633 nm. As has already been mentioned,

two peaks are needed to determine the index and the thickness, so the minimum thickness will be $\cong 500$ nm, given the substrates used.

The indices of the films were measured at the following wavelengths: 633, 780, and 1306 nm.

2.3 Nonlinear Response Characterization

2.3.1 Electric Field Induced Second Harmonic Generation

In this work, the NLO properties have been studied at the microscopic level for a large number of chromophores. It is a key characterization because the molecular properties are responsible for the nonlinear macroscopic response when the NLO chromophores are incorporated in the polymer systems. Besides, from a basic point of view, these measurements allow the results of calculations based on different theoretical models to be checked in the framework of NLO structure-properties relationship research. The theoretical background of these measurements is explained in [Chap. 1](#), in the section dedicated to EFISH, as well as in [Appendix B](#).

2.3.1.1 Experimental Setup

EFISH allows us to determine $\vec{\mu}_0 \vec{\beta}$, which is the scalar product of the molecule's dipole moment in the fundamental state with the vector part of the first-order hyperpolarizability tensor $\tilde{\beta}(-2\omega, \omega, \omega)$. The Maker fringes are obtained by measuring the second harmonic light generated by a solution where a static electric field is applied, and which moves in a perpendicular direction to the incident beam. $\vec{\mu}_0 \vec{\beta}$ is deduced from the intensity and spacing of these fringes.

The experimental setup for the SHG measurements in this work is shown schematically in [Fig. 2.7](#). The setup, as can be seen in the figure, consists of (a) a light source, (b) a NLO spectrometer and (c) a high-voltage generator, which are described in more detail below.

(a) Light source

The fundamental beam is generated by a Nd:YAG pulsed laser, Quantel “YG780 Q-switched”, which emits at wavelength $\lambda = 1064$ nm with a pulse duration of 8 ns and a maximum energy of 1 J/pulse. The of the laser beam, measured energy at the laser exit, used to make the measurements in this thesis was about 2 mJ/pulse. The frequency of repetition of the pumping lamps is 10 Hz.

In order to get light at 1.9 μm , the Nd:YAG beam is focused through a Raman cell, which consists of a 50 cm length tube in which high pressure hydrogen is locked (30 bar in this case). The stimulated Raman effect produces a shift in the incident beam frequency as a result of the vibrational mode excitation of the H_2

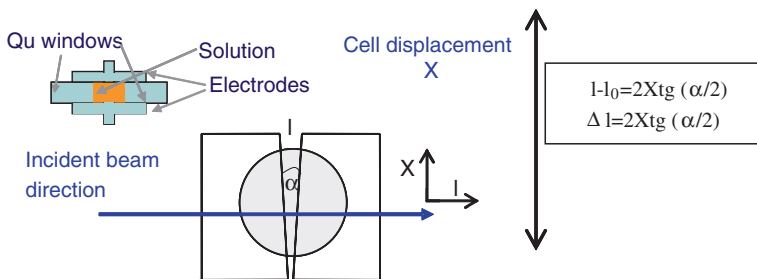


Fig. 2.9 Scheme of the cell for liquid measurements

a beam splitter, which directs approximately 10 % of the light intensity to a NPP (*N*-(4-nitrophenyl)-L-prolinol) sample. Suitable neutral filters are placed in front of the NPP sample as well as the lens that focuses the beam on it. The NPP is a non-centrosymmetric crystalline powder whose second harmonic signal is used as a reference to correct fluctuations of the light intensity of the laser. The intensity of the harmonic signal coming from the solution is divided by that obtained for the NPP. The rest of the light is directed towards the solution to be studied, passing through a half-wave ($\lambda/2$) plate, which allows us to turn the angle of the light polarization plane to adjust its intensity, and a Glan–Thompson polarizer, which determines the polarization of the excitation light (P^ω , parallel to the incident plane, which in our case is horizontal, and S^ω , perpendicular). For the EFISH measurements, the excitation light has to be vertically polarized, since the signal is much less intense for P^ω . The light is centred using a focusing lens in the cell containing the solution that we want to measure. The light coming from the sample passes through suitable interference filters (532 or 953 nm, full width at half maximum (FWHM) 20 nm) before reaching the detector.

In order to centre the sample as well as the reference, a He–Ne laser is used, at 633 nm. The He–Ne beam follows the same optical path as the excitation light of 1.06 or 1.91 μm .

The second harmonic generated by the sample and by the reference is detected using photomultipliers (Hamamatsu R2949 and R406), whose signal is integrated and later processed by the acquisition board (Keithley DAS 1600) incorporated in the computer.

(b2) Measurement cell

The cell where the solution to be measured is placed consists of two wedge-shaped quartz windows ($2 \times 1 \times 0.2 \text{ cm}^3$) forming a relatively small angle ($2\text{--}4^\circ$ for measurements at 1.06 μm and $5\text{--}7^\circ$ for measurements at 1.91 μm). The solution to be measured is then contained in the wedge-shaped space, and limited above and below by two electrodes (Fig. 2.9). The whole system is placed on a motorized platform, which moves in the direction perpendicular to the incident beam.

In order to determine the molecular hyperpolarizability of a compound in solution, it is necessary to know the solvent's hyperpolarizability, as it is a relative measurement. Therefore, in the experimental protocol we follow, the generated signal of the solvent is measured before and after each solution. This way, the long-term fluctuations that can be found in the laser intensity in a series of measurements are corrected. Each concentration is measured twice, as well as the solvent, the sequence solvent–solution–solvent being repeated at least three times. It is necessary to evaluate at least two different concentrations of each compound to rule out any possible mistake in the preparation of the solution. The typical process consists in the measurement of three solutions, although it is not unusual to need the measurement of several more.

(c) High voltage generator

In order to break the centrosymmetry of the considered solution, which is an isotropic liquid initially, the application of an electric field is needed. The electrical potential difference applied by a pulsed high voltage supply is at least 5–7 kV. The two electrodes are separated about 2 mm, and they are in contact with the quartz windows, and the solution. The pulsed character of the applied tension is necessary to avoid problems of hydrolysis and polarization in the solution. The pulse duration is 10 μ s. The high tension pulse is synchronized with the laser pulse, whose brief duration (8 ns) compared to that of the tension allows one to treat the system as if an electric static uniform field existed in the solution. The pulse is followed by means of an oscilloscope, which delivers a reading of the field applied to the solution, as it is possible to find slightly conductive solutions or those with a very high dielectric constant where the field experienced by the solution is less than the nominal one.

2.3.1.2 Data Treatment

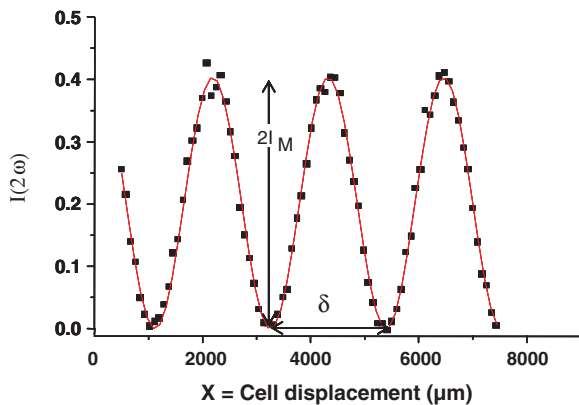
The experimental determination of the $\mu\beta_z$ product of a molecule is carried out in several steps. Measurements of the second harmonic intensity coming from the pure solvent are made to obtain $I^{2\omega}(0)$, alternating them with measurements of the solution at different concentrations x to obtain the coherence length $l_c(x)$ and $I^{2\omega}(x)$.

In the experiment, the Maker fringes are registered for a solution of the nonlinear molecule of interest in a certain solvent, that is, the oscillating function of $I^{2\omega}$ versus the light path, whose expression is reproduced in Equation B.15 (Appendix B):

$$I^{2\omega} = 2I_M \sin^2 \left(\frac{\pi l}{2l_c} \right) \quad (2.1)$$

where $2I_M$ is the amplitude of the fringes, which depends on the concentration, and l is the length travelled by the light in the liquid, related to the movement in the X transverse direction of the cell through

Fig. 2.10 Recording of the maker fringes obtained for a solution



$$I = 2X \tan(\alpha/2) + I_0 \quad (2.2)$$

where I_0 is the separation between the windows in the initial position (X_0) and α the angle between them.

In Fig. 2.10 a typical recording of the Maker fringes in EFISH is shown. The maximum amplitude of the fringes is identified as $2I_M$ and the spacing of the fringes as δ .

The curve (C.II) Eq. 2.1 can be fitted to the experimental data. In practice, we write it in a different way:

$$I^{2\omega} = 2A \left[1 - \cos \left(\frac{X}{B} + D \right) \right] \quad (2.3)$$

with A , B and D as fitting parameters.

A corresponds to the intensity I_M , B is related to the fringe spacing δ , which is the separation between two consecutive minima, by $\delta = 2\pi B$; and D is related to I_0 , representing the initial phase.

The coherence length, l_c , corresponds to the length in the liquid in which $I^{2\omega}$ grows. In Fig. 2.10, we can see that the cell displacement must be $\delta/2 = B\pi$, thus, substituting in Eq. 2.2, we have that

$$l_c = 2\pi B \tan(\alpha/2) \quad (2.4)$$

The l_c of the solvent we use is calculated from refractive index data that can be found in the literature. With this data, the first thing to do is to fit the fringes of the solvent to calculate the angle α that the windows form in the cell. In Table B.2 (Appendix B), all the parameters used for the measurement of the $\mu\beta$ of the molecules in this thesis are gathered. Let us see now how to obtain the nonlinear coefficient from the fitting parameters.

We start from Equation B.16 of Appendix B:

$$\sqrt{I_M^L} = C [\Gamma_L l_c - K] E_0,$$

where C and E_0 are given in the appendix and Γ_L is the macroscopic nonlinear susceptibility.

As was mentioned at the beginning of this section, the measurements are made by alternating them with measurements on the solvent, which are used as a reference, before and after each of the concentrations that are going to be evaluated. If x is the concentration of the solution, we have

$$\sqrt{I_M^L(x)} = C(\Gamma_L(x)l_c(x) - K)E_0(x) \quad (2.5)$$

If we divide the previous equation by its equivalent for $x = 0$ (pure solvent) and find the value of the susceptibility $\Gamma_L(x)$, we find

$$\Gamma_L(x) = \frac{1}{l_c(x)} \left[(l_c(0)\Gamma_L(0) - K) \sqrt{\frac{I_M^L(x)}{I_M^L(0)} \frac{E_0(0)}{E_0(x)}} + K \right] \quad (2.6)$$

We can see that it is possible to calculate $\Gamma_L(x)$ from the fitting parameters, and from the values of K gathered in Table B.1. In order to obtain $\mu\beta_z$, we have to deduce an expression that relates the macroscopic parameter $\Gamma_L(x)$ to the hyperpolarizabilities.

To this end, we will start by characterizing the concentration of the solution, x , as mass of solute, m_S , divided by the mass of solvent, m_D .

$$x = \frac{m_S}{m_D}$$

Therefore, we can write the number of molecules per volume unit of the solute and the solvent as

$$\begin{aligned} N_D &= \frac{\rho N_A}{M_D} \frac{1}{1+x} \\ N_S &= \frac{\rho N_A}{M_S} \frac{x}{1+x} \end{aligned} \quad (2.7)$$

where N_A is Avogadro's number and ρ the density of the solution, which we assume to be equal to that of the pure solvent because of the low concentration used.

The macroscopic nonlinear susceptibility is additive with respect to the contributions of the solvent and the solute, so from expression 1.32 we can write

$$\Gamma_{ZZZZ} = Nf\gamma^0 = f(N_D\gamma_D^0 + N_S\gamma_S^0) \quad (2.8)$$

and, substituting the expressions 2.7, we obtain that for the solution and the solvent

$$\Gamma_L(x) = \frac{\rho N_A f}{1+x} \left(\frac{\gamma_D^0}{M_D} + \frac{\gamma_S^0}{M_S} x \right) \quad (2.9)$$

By setting $x = 0$ in Eq. 2.9 we obtain the microscopic hyperpolarizability of the pure solvent:

$$\gamma_D^0 = \frac{\Gamma(0)M_D}{\rho N_A f} \quad (2.10)$$

Substituting Eq. 2.10 into Eq. 2.9 and finding the value for the hyperpolarizability of the solute, we obtain

$$\gamma_S^0 = \frac{M_S}{\rho N_A f x} [(1+x)\Gamma_L(x) - \Gamma_L(0)] \quad (2.11)$$

By retrieving now expression 1.33 and finding the value $\mu_0\beta_z$, we have

$$\mu_0\beta_z = \gamma^0 5kT \quad (2.12)$$

Therefore

$$\mu_0\beta_z = \frac{M_S 5kT}{\rho N_A f x} [(1+x)\Gamma_L(x) - \Gamma_L(0)] \quad (2.13)$$

To sum up, we can say that by using expressions 2.6 and 2.13 we can determine $\mu_0\beta_z$ from the amplitude of the recording of the intensity of the second harmonic induced by the electric field.

Calculation of $\mu\beta$ in cases where there is absorption

In order to calculate the static hyperpolarizability value, in many cases, and nearly always when working with dipole molecules under non-absorption-conditions at the fundamental and second harmonic frequencies, the two-level model is used, as was explained in Chap. 1. This magnitude is more representative for comparison purposes, since it is independent of the frequency of measurement. The expression used to calculate $\beta(0)$ is

$$\beta(0) = \beta(2\omega) \left[1 - 4 \left(\frac{\lambda_{\max}}{\lambda} \right)^2 \right] \left[1 - \left(\frac{\lambda_{\max}}{\lambda} \right)^2 \right] \quad (2.14)$$

where λ_{\max} is the maximum absorption wavelength of the compound in solution, and λ the measurement wavelength (1.06 μm , 1.9 μm).

In practice, the experimental data of the concentration and the A and B parameters from the fitting of Eq. 2.3 are entered in an Excel worksheet such as the one shown in Fig. 2.11, for more efficient treatment of the data.

Calculation of $\mu\beta$ in cases where there is absorption

In the data process described so far, the possibility that the solutions absorb the light used in the excitation (ω) or generated (2ω) has not been considered. Excitation at $\lambda = 1.9 \mu\text{m}$ avoids the absorption of the fundamental, but it is not unusual to find molecules with strong donor–acceptor substituents for which the absorption tail reaches 950 nm. Then it is very important to evaluate the absorption of the solution at 2ω , as this decreases the second harmonic intensity that we register, which leads us to underestimate the value of $\mu\beta$.

When the absorption spectrum of the molecules presents a slight absorption at the second harmonic of the measurement wavelength used in EFISH, the minima of the Maker fringes are not zero anymore, and the contrast of the oscillations decreases. The Maker fringes obtained thus were fitted to the following expression according to the model proposed by Oudar in 1977 [3]:

$$I^{2\omega} = 2OD \exp \left[- \left(\frac{\alpha_{2\omega} l}{2} \right) \right] \left[1 - \cos \left(\frac{X}{B} + D \right) \right] \quad (2.15)$$

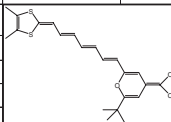
DATE:	12/18/2009	DAVID CELL							
$\lambda =$	1,907	microns	nwg=	1,44	G g E-14=	2,90			
$\tan(\alpha/2)=$	0,04925802		n2wg=	1,45					
SOLVENT		CH ₂ Cl ₂			MOLECULE				
nwl=	1,41	$\Gamma(0)$ E-14=	8,00	SERIES	ELL79				
n2wl=	1,41	lc (mic)=	136	MOL. W.=	420,6				
$\epsilon(0)=$	9,08	K E-14=	114,87	ABS(mic)=	0,546				
$\rho=$	1,3220	f local=	4,1973051						
FILE	x	A	B	HV (V)	lc (mic)	Γ (E-14)	gamma(E-34)	$\mu\beta$ (E-48)	$\mu\beta$ (0)(E-48)
EII7900-02	0	0,532	440,5	4,5	136,33	8			
EII7901	0,000427	1,11	436	4,5	134,94	11,29660885	97,31977021	1982,379389	1223,133186
						11,29660885	97,31977021	1982,379389	1223,133186
$\mu\beta(E-48)=$		1982	(esus)						
FILE	x	A	B	HV (V)	lc (mic)	Γ (E-14)	gamma(E-34)	$\mu\beta$ (E-48)	$\mu\beta$ (0)(E-48)
EII7902-04	0	0,525	438,6	4,5	135,75	8			
EII7903	0,000237	0,827	436,5	4,5	135,10	9,872095073	99,55166087	2027,842444	1251,184007
						9,872095073	99,55166087	2027,842444	1251,184007
$\mu\beta(E-48)=$		2028	(esus)						
Again c ₀									
FILE	x	A	B	HV (V)	lc (mic)	Γ (E-14)	gamma(E-34)	$\mu\beta$ (E-48)	$\mu\beta$ (0)(E-48)
EII7904-06	0	0,523	438	4,5	135,56	8			
EII7905	0,0004377	1,099	435,1	4,5	134,66	11,29058074	94,77074149	1930,456311	1191,096513
						11,29058074	94,77074149	1930,456311	1191,096513
$\mu\beta(E-48)=$		1930	(esus)						
$\mu\beta(E-48)=$		1980,2				$\mu\beta(0)(E-48)=$		1237,1586	

Fig. 2.11 Excel worksheet for the calculation of $\mu\beta$ from the values of A and B parameters measured experimentally

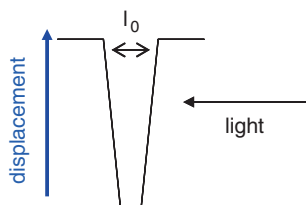


Fig. 2.12 Detail of the displacement of the quartz EFISH cell containing the solution

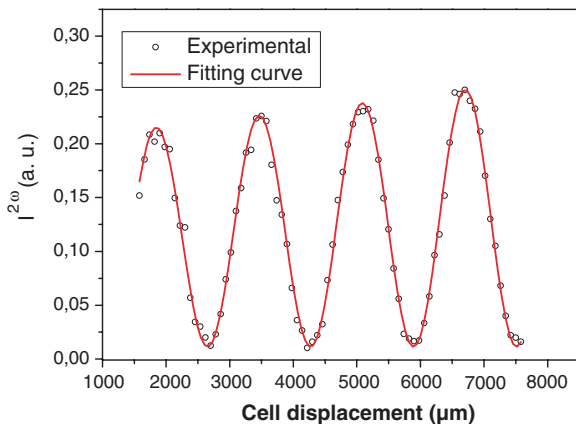
where $\alpha_{2\omega}$ is related to the optical density (or absorbance) as

$$\alpha_{2\omega} = \frac{OD \ln 10}{l} = \frac{A \cdot 2.303}{l} \quad (2.16)$$

The value of $\alpha_{2\omega}$ for each concentration used in EFISH is obtained by extrapolating from the coefficient of molar extinction, which is determined from the measurements of several more diluted concentrations prepared in an independent way.

By replacing l in the expression by its value, we obtain $l = l_0 - 2 \tan(\alpha/2)X$, which would imply a cell displacement in the way shown in Fig. 2.12.

Fig. 2.13 Maker fringes fitted to Eq. 2.17. for a solution showing absorption at 954 nm



The initial point of the trajectory has to be measured, as it is the distance between the two windows at that point. Thus, we would have the following expression to adjust the fringes and to obtain A and B by fixing $G = \alpha_{2\omega}/2$ and l_0 :

$$I^{2\omega} = A \exp \left[\left(l_0 - 2x \tan \frac{\alpha}{2} \right) (-G) \right] \left[1 - \cos \left(\frac{X}{B} + D \right) \right] \quad (2.17)$$

where $2X \tan \frac{\alpha}{2} \cong X \tan \alpha$ (if $\alpha < 10^\circ$).

Figure 2.13 shows a recording of Maker fringes for a solution showing absorption at the frequency of the second harmonic, together with the fit to the previous equation.

2.3.2 Thin Films: SHG in Thin Films Oriented by Corona Discharge

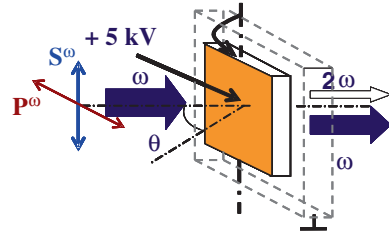
The SHG measurements described below allow the nonlinear coefficients that are the second-order susceptibility tensor ($\chi^{(2)}$) components to be obtained from the Maker fringe measurements.

Two kinds of polymer systems have been studied: side-chain liquid crystals (SCLCs) with donor- π -acceptor azo chromophores in the side chain, and mixtures of azo polymers with highly efficient nonlinear chromophores.

2.3.2.1 Experimental Setup

These measurements, as well as the ones for molecular characterization, require a light source, a nonlinear spectrometer, a continuous source of high voltage (to generate the field that breaks the film's) and different sample holders (rotating, with temperature control, etc.) for each kind of measurement. These are described in more detail below.

Fig. 2.14 Sample holder for the measurement of the Maker fringes in the oriented films



(a) Light source, spectrometer and cell

The light source and spectrometer used are like the ones described previously. All the measurements were made at $1.91 \mu\text{m}$, and basically two polarizations were used, P^ω (horizontal in our configuration) and S^ω (vertical).

Regarding the sample holder, several different ones have been used, designed according to the kind of measurements required and built in the workshop of the Condensed Matter Physics Department. One of them is a fixed and thermoregulated brass holder, which is placed in a position at 40° with respect to the incident laser direction. This way, the second harmonic signal can be monitored during the orientation produced by the poling.

Another sample holder used is a rotating one, which in a routine measurement turns $\pm 50^\circ$ around a vertical axis contained in the film, as shown in Fig. 2.14 (vertical axis). A third sample holder allows rotation around an axis perpendicular to the plane of the film and was used to measure the Maker fringes for different orientations of the film, as explained in Chap. 4.

(b) High voltage power supply. Polar orientation process by means of a field at high temperature

Thermal poling consists in orienting the sample by applying a field at high temperature and then cooling it down in the presence of the field to “freeze” the orientation. In our setup, a corona discharge is used, produced when a high voltage is applied between two conductors, at least one of which is sharp-shaped. This translates into a very intense electric field at the point, producing ionization of the surrounding air. The shape of the electrodes, distance, polarity and the gas present in the medium determine the particular features of the discharge. In our case, one of the electrodes (+) is a needle pointing towards the film. The film is placed on an ITO glass plate, which acts as the other electrode. The voltage applied to the edge of the approximately 1 mm diameter needle was between 5000 and 7000 V (see Fig. 2.15). The discharge between the needle and the film is discerned by light emission and a slight hiss. The positive ions produced seek a zone with a lower potential and reach the surface of the film (with a quite low conductivity). The distance between the electrodes (the edge of the needle and the surface of the film) is 1 cm.

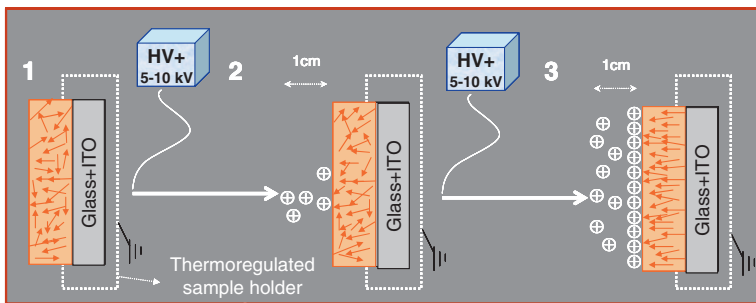


Fig. 2.15 Scheme of the orientation of the chromophores (*arrows* in the picture) by a corona discharge applied during the thermal poling

The polar molecules of a polymer film can be aligned this way, but only if the right temperature is reached so that they are sufficiently mobile ($\geq T_g$), so the process involves sample heating. This was performed in one of the holders previously described. The heating rate used was 5 °C/min, and the highest temperature reached was maintained for a period between 20 and 40 min, depending on the system studied. The cooling process was carried out with the field applied to “freeze” the orientation of the dipoles forced at high temperature [4]. A too-quick cooling process would result in the relaxation of the order achieved at high temperatures.

2.3.2.2 Data Treatment

The Maker fringe measurements are obtained with two polarizations of the excitation at frequency ω ($\lambda = 1.9 \mu\text{m}$): P^ω , which is parallel to the incident plane and S^ω , perpendicular to it. The polarization of the generated second harmonic light will depend, in general, on the symmetry of the system and the excitation light. The Maker fringes obtained from a quartz crystal (X-cut and in the usual configuration for measurements throughout this thesis) and for an oriented film (symmetry $C_{\infty v}$) with excitation light at 1.9 μm polarized in P^ω have the shape shown in Fig. 2.16a and b. In both cases, the nonlinear polarization is parallel to the incidence plane, so we will call it $P^{2\omega}$. Therefore, the notation for the configurations of the measurements will be $P^\omega P^{2\omega}$ and $S^\omega P^{2\omega}$.

As can be seen, the shape of the fringes is different from that obtained in the case of a solution, where all of them had the same height (Fig. 2.10). This is because the periodic variation of the sign, which is implied by the term $\sin^2(\Psi)$ (see Chap. 1), is modified in the case of solids by a projection factor $p(\theta)$, which is the main responsible for the envelope shape (amplitude variation) of the Maker fringes in solids, that we can see in the quartz (Fig. 2.16a). The thickness to work with, in the case of films is $\approx 1 \mu\text{m}$, while for quartz crystal it is $\approx 1 \text{ mm}$. Thus, in the case of quartz, we see more than one maximum, because the light covers a distance in the material several times the coherence length. However, for thin films, when turning between -50° and $+50^\circ$ the first maximum cannot be seen.

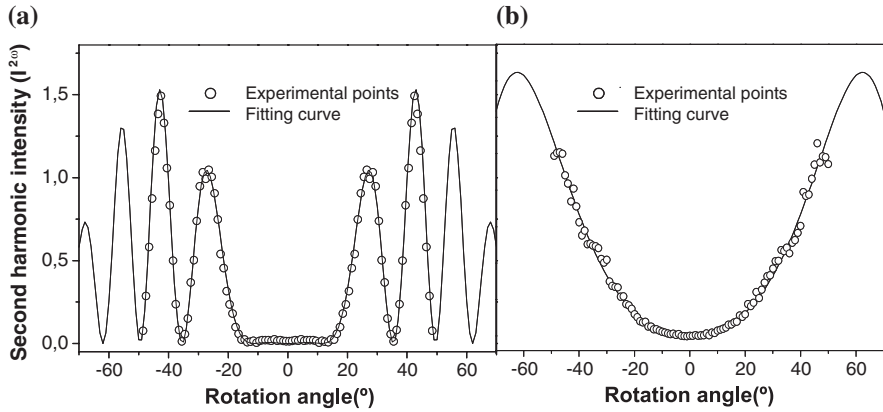


Fig. 2.16 Maker fringes for quartz glass a and for (a) polymeric thin film from this research (b)

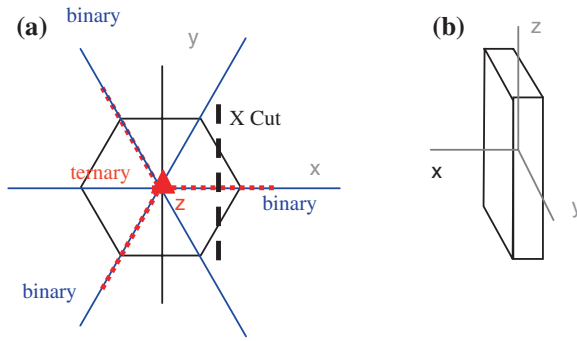


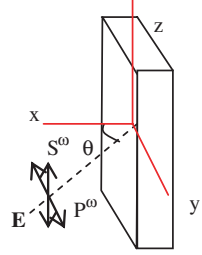
Fig. 2.17 X-cut quartz crystal. Symmetry elements

The determination of the nonlinear coefficients of the films is made from the measurements of the $I^{2\omega}$ of the sample, with respect to that generated by quartz glass. The expression that we will have to adjust to the experimental data and which allows us to find the value of the nonlinear coefficients is the one proposed by Jerphagnon and Kurtz [5] for quartz and, in general, for systems with low anisotropy values, and Herman and Hayden's one for highly birefringent films.

In this thesis, the nonlinear response of materials with different symmetry has been analysed: the X-cut quartz already mentioned (see Fig. 2.17) and polymeric thin films with uniaxial and biaxial polar orientation. Below, the features of the different experimental configurations will be detailed. Throughout, second-order nonlinear coefficients were used, d_{ijk} , whose relationship to the second-order susceptibility is given here as a reminder:

$$d_{ijk} = \chi_{ijk}/2.$$

Fig. 2.18 Measurement configuration for maker fringes for a quartz crystal



(a) For a quartz crystal

Quartz belongs to the trigonal point group 32 (international notation) or D_3 (Schoenflies notation), so we will find a ternary axis (optical axis) and three binary ones (see Fig. 2.17a) as symmetry elements. X-cut crystals are cut with the large faces perpendicular to the binary X-axis and the turns are made around the ternary Z-axis, Fig. 2.17b.

For this crystal, the only nonzero nonlinear coefficients are $d_{12} = -d_{11} = d_{26}$ and $d_{25} = -d_{14}$. As $d_{14} \ll d_{11}$, the relationship between the polarization and the fields that generate it is written as

$$\begin{pmatrix} P_x^{(2)} \\ P_y^{(2)} \\ P_z^{(2)} \end{pmatrix} = \begin{pmatrix} d_{11} & -d_{11} & 0 & 0 & 0 & 0 \\ 0 & 0 & 0 & 0 & 0 & -d_{11} \\ 0 & 0 & 0 & 0 & 0 & 0 \end{pmatrix} \begin{pmatrix} E_x^2 \\ E_y^2 \\ E_z^2 \\ 2E_y E_z \\ 2E_x E_z \\ 2E_x E_y \end{pmatrix}$$

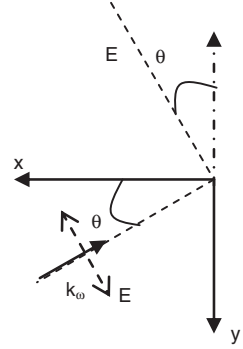
As the value of d_{11} is known (0.35 pm/V at 1.9 μm and 0.45 pm/V at 1.06 μm), we can use the second harmonic signal of this sample to scale the intensity obtained for samples whose NLO coefficients are unknown.

Since this material hardly shows dispersion, and its birefringence is small, we can apply the JK model (Appendix A) to fit the fringes obtained experimentally. We will use $I^{2\omega}$ measurements of the crystal in the orientation that is shown in Fig. 2.18. Therefore

$$I_{2\omega}'' = \left(\frac{8\pi c}{((n^\omega)^2 - (n^{2\omega})^2)^2} \right) d^2 p^2(\theta) |E'_\omega|^4 t_\omega'^4 T_{2\omega}'' \sin^2 \psi, \quad (2.18)$$

where d^2 represents the nonlinear effective coefficient of the sample, whose shape depends on the precise configuration of the measurement. In this expression we know all the parameters except for the incident electric field amplitude, which will be the same for the measurement of any sample, as for the reference quartz.

Fig. 2.19 Scheme of the incidence of the excitation light on the sample



1. If the polarization of the incident light is parallel to the plane of incidence (P^ω in the picture), the components of the excitation field will be

$$E = (E_x, E_y, 0) = (E \sin \theta, -E \cos \theta, 0)$$

By substituting this in Equation A and developing the expression, we have that

$$P_x = d_{11} E^2 \sin^2 \theta'_\omega - d_{11} E^2 \cos^2 \theta'_\omega = -d_{11} E^2 \cos 2\theta'_\omega,$$

$$P_y = 2d_{11} E^2 \sin \theta'_\omega \cos \theta'_\omega = d_{11} E^2 \sin 2\theta'_\omega,$$

$$P_z = 0.$$

We see that the $P^{2\omega}$ nonlinear polarization is contained in the xy -plane, the incidence plane, so we will name this configuration $P^\omega P^{2\omega}$.

As we have defined η (see Appendix A), in the case of Fig. 2.19 it would be the angle formed by the nonlinear polarization and the $-y$ -axis, which would be $-(\pi/2 + 2\theta'_\omega)$, as we infer from the expressions for P_x and P_y .

The projection factors will have then the following form:

$$p_1 = 1,$$

$$p_2 = \cos(\theta'_\omega - \eta) = \cos(3\theta'_\omega + \pi/2) = -\sin 3\theta'_\omega$$

$$\text{Then: } p^2(\theta) = \sin^2 3\theta'_\omega.$$

On the other hand, the harmonic and the fundamental wave are polarized perpendicular to the optical axis so, in the calculations, only the ordinary refractive index will be involved, both at the fundamental frequency n_o^ω and at the harmonic one $n_o^{2\omega}$.

2. If the polarization of the incident light is perpendicular to the incidence plane (S^ω in the picture), the E field would have just a Z component, that is, $E = (0, 0, E)$. In this case, it is very quick to check, by substituting in Equation A, that the three components of the nonlinear polarization are zero, $P_L^{(2\omega)} = 0$, so there is no nonlinear response for this configuration.

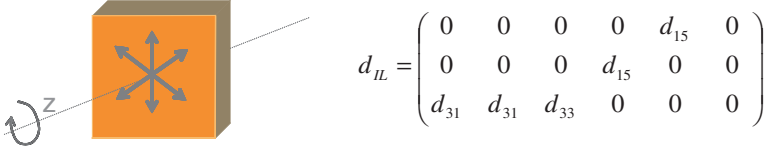


Fig. 2.20 Illustration of the symmetry a film acquires by poling orientation

(b) For an oriented film

In the case of polymeric films oriented by an electric field, two different situations have been studied. The thermal poling method, already described, applied to initially isotropic samples, leads to uniaxial systems of $C_{\infty v}$ symmetry with the axis perpendicular to the plane of the film. However, the use of photoassisted processes can vary that symmetry, giving rise, for example, to biaxial films with orientations compatible with C_{2v} symmetry.

As the medium is dispersive and the birefringence in some of the films is quite high (Δn up to 0.3), we use Equation A.71 (Appendix A) from the model proposed by HH for the second harmonic power at the exit of a uniaxial film, which is

$$P_{2\omega} = \frac{128\pi^3}{cA} d_{eff}^2 \left(\frac{n^{2\omega l}}{n^{2\omega}} \right)^4 \left(\frac{(n^\omega)^2 - (n^{2\omega})^2}{(n^\omega)^2 - (n^{2\omega l})^2} \right) \sin^2 \psi$$

$$\frac{[t_{\omega}^{a \rightarrow m}]^4 [T_{2\omega}^{m \rightarrow s}]^2 [T_{2\omega}^{s \rightarrow a}]^2}{\cos^2 \gamma_{2\omega} \cos^2 (\theta'_{2\omega} - \gamma_{2\omega}) (n^\omega \cos \theta'_\omega - n^{2\omega} \cos \theta'_{2\omega})^2} P_\omega^2$$

where d_{eff} is the effective nonlinear coefficient, which includes the projection factor and the nonlinear coefficient, and the index expression for the bound wave is

$$n^{2\omega l}(\theta'_\omega) = n^\omega \left(\frac{1}{\frac{\sin^2 \theta}{(n_e^{2\omega})^2} + \frac{(n^\omega)^2 - \sin^2 \theta}{(n_o^{2\omega})^2}} \right)^{1/2},$$

as explained in the [Chap. 1](#) of this report.

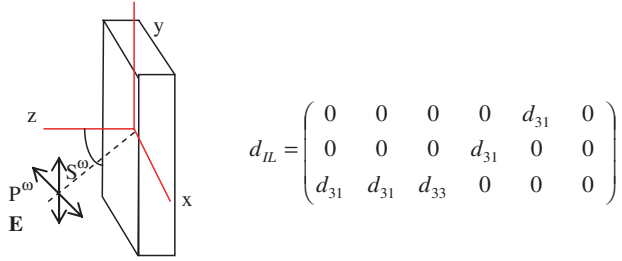
In the previous expression, the effective indices and coefficients have to be distinguished for the two configurations of measurement $S^\omega P^{2\omega}$ and $P^\omega P^{2\omega}$.

(b1) Uniaxial films. Point group ∞mm (international notation), $C_{\infty v}$ (Schoenflies notation)

In the most common case of thin films oriented by a field, the C_∞ symmetry axis is the one perpendicular to its surface. In this case, the d_{IL} tensor is as given in [Fig. 2.20](#).

By applying the Kleinman symmetry condition, we know that $d_{15} = d_{31}$, so there are only two independent coefficients, d_{31} and d_{33} ([Fig. 2.21](#)).

Fig. 2.21 Scheme of incidence of the excitation light on the uniaxially oriented film



We define the film axes such that the z -axis matches the optical one (normal to the film), which is perpendicular to the incidence plane. We will make the film turn around the y -axis (Fig. 2.21).

1. If the polarization of the incident light is perpendicular to the plane of incidence (XZ) S^ω :

$$E = (0, E, 0),$$

$$\begin{pmatrix} P_x^{(2)} \\ P_y^{(2)} \\ P_z^{(2)} \end{pmatrix} = \begin{pmatrix} 0 & 0 & 0 & 0 & d_{31} & 0 \\ 0 & 0 & 0 & d_{31} & 0 & 0 \\ d_{31} & d_{31} & d_{33} & 0 & 0 & 0 \end{pmatrix} \begin{pmatrix} 0 \\ E^2 \\ 0 \\ 0 \\ 0 \\ 0 \end{pmatrix} \quad \left| \begin{array}{l} P_x = 0 \\ P_y = 0 \\ P_z = d_{31} E^2 \end{array} \right.$$

The polarization is in the plane of incidence, so the measurement configuration will be $S^\omega P^{2\omega}$. Regarding the $p(\theta) = p_1 p_2$ factor, we have that

$$p_1 = 1,$$

since $|P'_{2\omega}| = p_1 d |E'_\omega|^2$, and for $P^{2\omega}$ we have

$$p_2 = \left[\cos \left((\theta'_{2\omega} - \gamma_{2\omega}) - \eta \right) \right]$$

because $\theta'_\omega \neq \theta'_{2\omega}$, where η , in this case, is the angle between $P^{2\omega}$ and the film surface, or x -axis in the figure, which is 90° , because it goes along the z direction. Thus

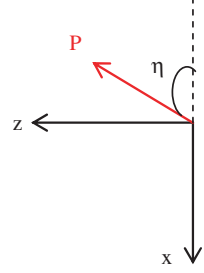
$$(p_1 p_2)^2 = \sin^2 (\theta'_{2\omega} - \gamma_{2\omega}),$$

$$d_{eff}^2 = d_{31}^2 \sin^2 (\theta'_{2\omega} - \gamma_{2\omega}).$$

The refractive index for the fundamental wave will be n_o^ω (perpendicular to the optical axis) and for the harmonic one it will be $n^{2\omega}(\theta)$, which, considering the ellipsoid of indices for the frequency 2ω (Fig. 1.5), will have the expression

$$\left(n^{2\omega}(\theta) \right)^2 = (n_o^{2\omega})^2 + [1 - (n_o^{2\omega})^2 / (n_e^{2\omega})^2] \sin^2 \theta.$$

Fig. 2.22 η angle for P^ω excitation light in uniaxial films



The intensity generated by the film in this configuration depends only on the parameter d_{31} , which can be obtained by fitting the experimental data to Equation A.71 (the refractive indices and the thickness of the sample are known).

2. If the polarization of the incident light is parallel to the plane of incidence P^ω :

$$E = (-E \cos \theta, 0, E \sin \theta),$$

$$\begin{pmatrix} P_x^{(2)} \\ P_y^{(2)} \\ P_z^{(2)} \end{pmatrix} = \begin{pmatrix} 0 & 0 & 0 & 0 & d_{31} & 0 \\ 0 & 0 & 0 & d_{31} & 0 & 0 \\ d_{31} & d_{31} & d_{33} & 0 & 0 & 0 \end{pmatrix} \begin{pmatrix} E^2 \cos^2 \theta'_\omega \\ 0 \\ E^2 \sin^2 \theta'_\omega \\ 0 \\ -2E^2 \sin \theta'_\omega \cos \theta'_\omega \\ 0 \end{pmatrix},$$

$$P_x = -2d_{31}E^2 \sin \theta'_\omega \cos \theta'_\omega = -d_{31} \sin 2\theta'_\omega,$$

$$P_y = 0,$$

$$P_z = d_{31}E^2 \cos^2 \theta'_\omega + d_{33}E^2 \sin^2 \theta'_\omega$$

The nonlinear polarization is parallel to the plane of incidence, so we have a $P^\omega P^{2\omega}$ configuration. We have to consider, besides, the walk-off angle for θ'_ω and $\theta'_{2\omega}$, given that the medium is birefringent and the dispersion is important (see Chap. 1):

$$(p_1 d)^2 = \left[d_{31} \sin(2\theta'_\omega - \gamma_\omega) \right]^2 + \left[d_{31} \cos^2(\theta'_\omega - \gamma_\omega) + d_{33} \sin^2(\theta'_\omega - \gamma_\omega) \right]^2,$$

$$p_2 = \cos((\theta'_{2\omega} - \gamma_{2\omega}) - \eta) = \cos(\theta'_{2\omega} - \gamma_{2\omega}) \cos \eta + \sin(\theta'_{2\omega} - \gamma_{2\omega}) \sin \eta$$

where $\eta = \arctan(P_z/P_x)$ (Fig. 2.22), so we know

$$\tan \eta = P_z/P_x$$

By applying the identity:

$$\tan^2 \eta + 1 = \sec^2 \eta$$

We have that

$$\begin{aligned}\sin \eta &= \frac{\tan \eta}{(1 + \tan^2 \eta)^{1/2}}, \\ \cos \eta &= \frac{1}{(1 + \tan^2 \eta)^{1/2}}, \\ \sin \eta &= \frac{d_{31} \cos^2(\theta'_\omega - \gamma_\omega) + d_{33} \sin^2(\theta'_\omega - \gamma_\omega)}{[d_{31}^2 \sin^2(2\theta'_\omega - \gamma_\omega) + (d_{31} \cos^2(\theta'_\omega - \gamma_\omega) + d_{33} \sin^2(\theta'_\omega - \gamma_\omega))^2]^{1/2}}, \\ \cos \eta &= \frac{d_{31} \sin(2\theta'_\omega - \gamma_\omega)}{[d_{31}^2 \sin^2(2\theta'_\omega - \gamma_\omega) + (d_{31} \cos^2(\theta'_\omega - \gamma_\omega) + d_{33} \sin^2(\theta'_\omega - \gamma_\omega))^2]^{1/2}}\end{aligned}$$

By introducing $\sin \eta$ and $\cos \eta$ in p_2 :

$$p_2 = \frac{\sin(\theta'_{2\omega} - \gamma_{2\omega})[d_{31} \cos^2(\theta'_\omega - \gamma_\omega) + d_{33} \sin^2(\theta'_\omega - \gamma_\omega)] + \cos(\theta'_{2\omega} - \gamma_{2\omega})d_{31} \sin(2\theta'_\omega - \gamma_\omega)}{[d_{31}^2 \sin^2(2\theta'_\omega - \gamma_\omega) + (d_{31} \cos^2(\theta'_\omega - \gamma_\omega) + d_{33} \sin^2(\theta'_\omega - \gamma_\omega))^2]^{1/2}}$$

which results in,

$$\begin{aligned}d_{eff}^2 &= [dp(\theta)]^2 = (dp_1)^2 p_2^2 = \sin(\theta'_{2\omega} - \gamma_{2\omega})[d_{31} \cos^2(\theta'_\omega - \gamma_\omega) \\ &\quad + d_{33} \sin^2(\theta'_\omega - \gamma_\omega)] + \cos(\theta'_{2\omega} - \gamma_{2\omega})d_{31} \sin(2\theta'_\omega - \gamma_\omega)\end{aligned}$$

Regarding the refractive indices, we have to consider the ellipsoid for the fundamental wave and for the harmonic. The index for the bound harmonic wave is defined in Appendix A as

$$\begin{aligned}(n^\omega(\theta))^2 &= (n_o^\omega)^2 + [1 - (n_o^\omega)^2/(n_e^\omega)^2] \sin^2 \theta, \\ (n^{2\omega}(\theta))^2 &= (n_o^{2\omega})^2 + [1 - (n_o^{2\omega})^2/(n_e^{2\omega})^2] \sin^2 \theta.\end{aligned}$$

In this case, the intensity of the generated second harmonic depends on d_{31} and d_{33} . By using the value of d_{31} obtained from the $S^\omega P^{2\omega}$ measurement, it is possible to find the value of d_{33} by fitting the measured data in $P^\omega P^{2\omega}$ to the expression.

(b2) Biaxial films. Point group 2 *mm* (international notation), C_{2v} (Schoenflies notation)

Irradiation with linearly polarized UV light makes the chromophores orient preferably in a perpendicular plane, so when an electric field is applied, the typical configuration of a single axis perpendicular to the film and equality in all directions in the plane of the film is changed.

For films oriented this way, there would be a Z-axis, perpendicular to the film and which matches the direction of the electric field orienting the dipoles, and two non-equivalent X- and Y-axes in the plane, one of which (Y) coincides with the polarization direction of the UV light. The chromophores would be, therefore, preferably in the XZ plane. In Fig. 2.23 this situation is represented in a schematic way.

Fig. 2.23 Scheme of the axes for a film oriented by irradiation with polarized light and thermal poling

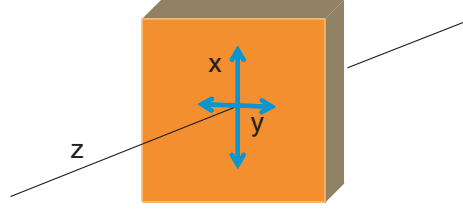
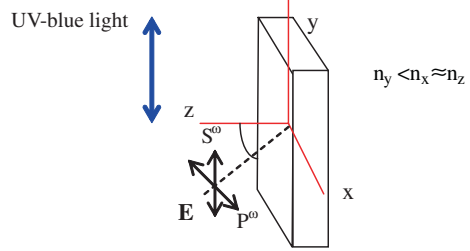


Fig. 2.24 Scheme of incidence of the excitation light in the biaxially oriented film. The irradiation direction is also marked



The components of the nonlinear susceptibility tensor would be d_{31} , d_{32} , d_{33} , d_{24} and d_{15} , and by applying Kleinman symmetry conditions ($d_{15} = d_{31}$, $d_{32} = d_{24}$), we find the tensor has the form [6]

$$d_{IL} = \begin{pmatrix} 0 & 0 & 0 & 0 & d_{31} & 0 \\ 0 & 0 & 0 & d_{24} & 0 & 0 \\ d_{31} & d_{24} & d_{33} & 0 & 0 & 0 \end{pmatrix}$$

In this case, the measurements of the Maker fringes will not be equivalent when turning around the perpendicular axis of the film (Z).

Orientation 1 (Fig. 2.24):

1. Perpendicular polarization of the incident light: S^ω

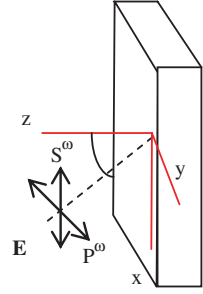
$$E = (0, E, 0),$$

$$\begin{pmatrix} P_x^{(2)} \\ P_y^{(2)} \\ P_z^{(2)} \end{pmatrix} = \begin{pmatrix} 0 & 0 & 0 & 0 & d_{31} & 0 \\ 0 & 0 & 0 & d_{24} & 0 & 0 \\ d_{31} & d_{24} & d_{33} & 0 & 0 & 0 \end{pmatrix} \begin{pmatrix} 0 \\ E^2 \\ 0 \\ 0 \\ 0 \\ 0 \end{pmatrix} \quad \left| \begin{array}{l} \text{As } d_{24} = d_{32}, \\ P_x = 0 \\ P_y = 0 \\ P_z = d_{24}E^2 \end{array} \right.$$

Therefore, we have an $S^\omega P^{2\omega}$ configuration. The process to obtain the projection factors is analogous to the situation for a uniaxial film, except for the fact that the coefficient that matters is d_{24} , instead of d_{31} , and that the refractive indices will be the following: For the fundamental wave, n_y^ω (perpendicular to the optical axis z), and for the harmonic,

$$\left(n^{2\omega}(\theta) \right)^2 = (n_x^{2\omega})^2 + [1 - (n_x^{2\omega})^2 / (n_z^{2\omega})^2] \sin^2 \theta$$

Fig. 2.25 Scheme of incidence of the excitation light in a biaxially oriented film, with the orientation perpendicular to the irradiation



2. Parallel polarization of the incident light: P^ω

We have the same projection factors as in the case of the $P^\omega P^{2\omega}$ configuration, and the same coefficients, d_{33} and d_{31} , are involved. The refractive indices are

$$\begin{aligned} (n^\omega(\theta))^2 &= (n_o^\omega)^2 + [1 - (n_o^\omega)^2 / (n_e^\omega)^2] \sin^2 \theta, \\ (n^{2\omega}(\theta))^2 &= (n_o^{2\omega})^2 + [1 - (n_o^{2\omega})^2 / (n_e^{2\omega})^2] \sin^2 \theta. \end{aligned}$$

Orientation 2 (Fig. 2.25):

1. Perpendicular polarization of the incident light: S^ω

$$\begin{aligned} E &= (E, 0, 0), \\ P_x &= 0, \\ P_y &= 0, \\ P_z &= d_{31} E^2. \end{aligned}$$

The configuration is the same as in the uniaxial case, giving the same projection factors. The equation of the second harmonic intensity will give us the value of d_{31} , so, with this value and together with the $P^\omega P^{2\omega}$ measurement configuration in the other orientation, we find the value of d_{33} .

The refractive index for the fundamental wave is n_x^ω (perpendicular to the optical axis z) and for the harmonic one it is n_x^ω (parallel to the optical axis z).

2. Parallel polarization of the incident light: P^ω

$$\begin{aligned} E &= (E, -E \cos \theta, E \sin \theta), \\ P_x &= 0, \\ P_y &= -2d_{24} E^2 \sin \theta'_\omega \cos \theta'_\omega = -d_{24} \sin 2\theta'_\omega, \\ P_z &= d_{24} E^2 \cos^2 \theta'_\omega + d_{33} E^2 \sin^2 \theta'_\omega. \end{aligned}$$

The configuration of the measurement will be $P^\omega P^{2\omega}$, and given the value of d_{24} calculated by using the other orientation in $S^\omega P^{2\omega}$ configuration, it will be possible to calculate d_{33} , and to confirm the value found before. The projection factors will be analogous to those obtained for this configuration in the other orientation.

The refractive indices are

$$\begin{aligned} \left(n^\omega(\theta)\right)^2 &= (n_y^\omega)^2 + [1 - (n_y^\omega)^2 / (n_z^\omega)^2] \sin^2 \theta, \\ \left(n^{2\omega}(\theta)\right)^2 &= (n_y^{2\omega})^2 + [1 - (n_y^{2\omega})^2 / (n_z^{2\omega})^2] \sin^2 \theta. \end{aligned}$$

2.4 Nonlinear Gratings

A NLO grating is a system in which the nonlinear susceptibility shows a periodic spatial modulation. The devices based on these gratings are of particular interest because they can generate second harmonic diffracted beams, which can be spatially separated from the excitation light [7]. Organic mesostructured materials with NLO properties have potential applications in photonics, as compact diode laser sources, or as waveguides [8].

In this work, the preparation of NLO gratings is based on providing a diffraction grating (previously induced by means of light irradiation) with NLO properties. First of all, we will briefly describe the formation of the gratings and then we will focus on their polar orientation.

2.4.1 Recording of Diffraction Gratings

Two monochromatic plane waves of coherent linearly polarized light are made to interfere, thus generating a periodic modulation (interference pattern) in the intensity. In the cases addressed by this thesis, linearly polarized light of 406 and 488 nm was used. If the overlapping of the two beams takes place on a photo addressable material, as in the case of polymers comprising azobenzene units, the refractive index of the film will be modified selectively, as the zones affected by light will be oriented, as we have seen before, by the so-called Weigert effect, and the dark zones will not.

In Fig. 2.26, a scheme of diffraction-grating recording is shown.

When a light beam strikes the optically recorded zone, besides the direct beam that passes directly through the sample, the diffraction maxima, which will depend on the recorded pattern, will be observed.

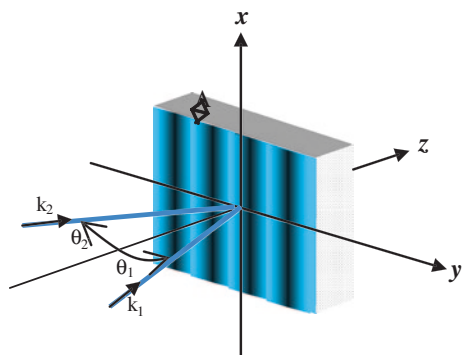
The intensity modulation period that is created on the plane of a thin film depends on the angle between the two beams and their wavelength (λ_g) as

$$\Lambda = \frac{\lambda_g}{\sin \theta_1 + \sin \theta_2}. \quad (2.19)$$

If we irradiate this recorded grating with a beam with wavelength λ , we will obtain, as we said before, various diffraction maxima at some specific angles. If we irradiate the grating at an angle θ_{in} , the generated diffracted maximum of order m will be appear at an angle given by

$$\sin \theta_m = \frac{m\lambda}{\Lambda} + \sin \theta_{in}. \quad (2.20)$$

Fig. 2.26 Scheme of the interference of two beams on a film to create a diffraction grating



In order to characterize the grating, the diffraction efficiency is usually calculated as the incident light power fraction that appears in each diffraction order.

Besides the previously described recording of the gratings based on a periodic modulation of the refractive index, when an azopolymer film is irradiated with an interference pattern a modification of the surface relief takes place. This modification consists in the modulation of the film thickness with the same period as that of the interference of the two beams [9]. In this way, relief gratings with periods on the micrometre scale, and surface modulations of hundreds of nanometres can be achieved. The relief in these gratings can be increased by heating the films to temperatures in the mesophase range.

The formation of the surface relief is due to polymeric chain migrations happening on a large scale, because of the photoinduced spatial anisotropy together with a component of the electric field gradient. The presence of azobenzene side groups is a critical structural requirement for the surface distortion process. Moreover, the strong donor–acceptor structure of the main chain is also helpful, as its excited “*cis*” state shows a shorter half-life, so there are more cycles on the same time scale. On the other hand, LCs show some advantages in the recording process because they reach a higher degree of photoinduced anisotropy [10].

Among the theories developed to understand the process of formation of this surface relief, one claims that the movements in the polymeric chains are due to the pressure gradients generated when the required volume increases during azobenzene isomerization. Thus, the mass would migrate from the zones undergoing photoisomerization (irradiated zones) to those where there is less or no isomerization (dark zones). However, another theory says that the interaction between the oriented polar molecules generates an attractive force that makes molecules migrate to more ordered domains, and so an increase in relief occurs in the irradiated zones [11]. On the other hand, there are also studies in LCPs, which are similar to the ones we are going to deal with in this thesis, in which surface relief maxima in the irradiated zones were found depending on the pulsed laser power used for the recording. Thus, below a certain value of the light power the irradiated zones show maxima and above it they show depressions, assigned to polymer ablation [12].

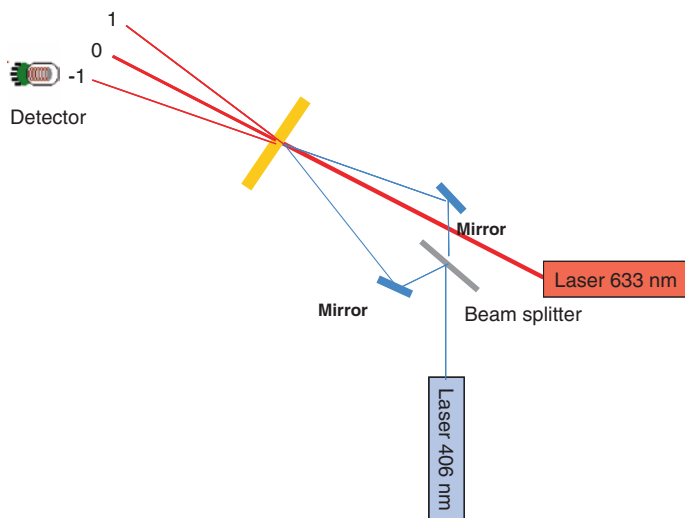


Fig. 2.27 Scheme of the experimental setup for recording nonlinear gratings

2.4.2 Recording of Nonlinear Gratings

Nonlinear relief gratings are particularly interesting, because they separate automatically the second harmonic wave from the fundamental one. On the other hand, one of the problems in achieving the maximum efficiency of the nonlinear effects in a bulk material arises from the phase difference between the fundamental wave and the harmonics, caused by dispersion. In the particular case of SHG, it is very difficult to achieve the “phase matching” condition (the efficiency of the phenomenon would be maximum then) by using only the anisotropy in the material. An alternative way to obtain large efficiencies is by introducing a periodic modulation of the susceptibility tensor in the material, with a periodicity equal to the coherence length of the waves interacting in it [13]. As we have seen before, the modulation period of the grating can be chosen by adjusting the incidence angles of the blue light used to record the grating (Eq. 2.19.).

The experimental setup used to record the relief gratings with light at 406 nm is shown in Fig. 2.27. As can be seen, the light from a diode laser at 406 nm and maximum power of 20 mW is split into two beams, which are overlapped in the film by using two mirrors, thus creating an interference pattern. In order to check whether the grating is being recorded, the recorded area is irradiated with a He–Ne beam to observe the diffraction maxima; a detector is placed in one of the first diffraction maxima with the aim of monitoring the process.

NLO properties can be induced in the grating by applying an electric field at the same time as the grating is recorded, in what would be a photoassisted poling process. Another effective method is to apply thermal poling to the grating afterwards.

The nonlinear grating efficiency is characterized by applying a horizontally polarized (P^o) laser beam at 1.064 μm with an incidence angle of about 40° . The second harmonic generated light intensity at 532 nm will be detected by a Hamamatsu photomultiplier, with suitable interference filters to remove light at other wavelengths. Thus, for each film, up to three diffraction maxima intensities are measured. In order to characterize the nonlinear grating efficiency the intensity ratio of the first- and zero-order diffracted harmonic light is calculated.

References

1. R. Alicante et al., Synthesis and nonlinear optical properties of side chain liquid crystalline polymers containing azobenzene push-pull chromophores. *J. Polym. Sci. Part A: Polym. Chem.* **48**(1), 232 (2010)
2. R. Ulrich, R. Torge, Measurement of thin film parameters with a prism coupler. *Appl. Opt.* **12**(12), 2901 (1973)
3. J.L. Oudar, Optical nonlinearities of conjugated molecules. Stilbene derivatives and highly polar aromatic compounds. *J. Chem. Phys.* **67**(2), 446 (1977)
4. D. S. Chemla, Z. Zyss (Eds.) *Nonlinear Optical Properties of Organic Molecules and Crystals* (Academic Press, New York, 1987) 1
5. J. Jerphagnon, S.K. Kurtz, Maker fringes: a detailed comparison of theory and experiment for isotropic and uniaxial crystals. *J. Appl. Phys.* **41**(4), 1667 (1970)
6. F. Zernicke, J.E. Midwinter, *Applied Nonlinear Optics* (Wiley, New York, 1973)
7. L.M. Blinov et al., Polar diffraction gratings made by spatially periodic photopoling Langmuir–Blodgett films. *Appl. Phys. Lett.* **80**(1), 16 (2002)
8. Y. Che et al., Fabrication of surface relief grating with second-order nonlinearity using urethane-urea copolymer films. *Jpn. J. Appl. Phys., Part 1* **38**(11), 6316 (1999)
9. N.K. Viswanathan et al., Surface relief structures on azo polymer films. *J. Mater. Chem.* **9**(9), 1941 (1999)
10. T.G. Pedersen et al., Mean-field theory of photoinduced formation of surface reliefs in side-chain azobenzene polymers. *Phys. Rev. Lett.* **80**(1), 89 (1998)
11. T.G. Pedersen, P.M. Johansen, Mean-field theory of photoinduced molecular reorientation in azobenzene liquid crystalline side-chain polymers. *Phys. Rev. Lett.* **79**(13), 2470 (1997)
12. F.J. Rodríguez, Ph.D. Dissertation, Propiedades ópticas fotoinducidas en polímeros con unidades de azobenceno Universidad de Zaragoza, 2005
13. G. Martin et al., Photo-induced non-linear susceptibility patterns in electro-optic polymers. *Synth. Met.* **127**(1–3), 49 (2002)

Photoinduced Modifications of the Nonlinear Optical
Response in Liquid Crystalline Azopolymers

Alicante, R.

2013, XX, 200 p., Hardcover

ISBN: 978-3-642-31755-2